Experimental and numerical study of the dispersion of motor vehicle pollutants under idle condition

Z. Ning[a], C.S. Cheung[b,*], Y. Lu[a], M.A. Liu[b], W.T. Hung[c]

[a]*College of Mechanical and Electrical Engineering, Beijing Jiaotong University, Beijing 100044, PRChina*
[b]*Department of Mechanical Engineering, The Hong Kong Polytechnic University, Hung Hom, Kowloon, Hong Kong SAR, PRChina*
[c]*Department of Civil and Structural Engineering, The Hong Kong Polytechnic University, Hung Hom, Kowloon, Hong Kong SAR, PRChina*

Abstract

The aim of the work presented here is to study experimentally and numerically the dispersion characteristics of vehicular exhaust plume at an idle condition in an idealized and simplified environment. The gaseous and particulate concentrations in the exhaust plume of three idling motor vehicles were measured in an isolated environment under calm weather conditions. Despite the difference in the initial concentrations, the pollutants decayed exponentially in all directions.

The CFD code PHOENICS 3.3, with the $k–\varepsilon$ eddy dissipation sub-model, was used for the numerical simulation. The simulated results match very well with the experimental results close to the source of emission but decay to the ambient concentrations much slower. The effects of the initial emission concentration, exit velocity, exit direction and crosswind intensity have been investigated parametrically. The initial pollutant concentration will increase the local concentrations but the pattern of dispersion remains the same. The exit velocity will increase the momentum of the jet, resulting in a deeper penetration downstream. The exit angle has a stronger influence on pollutant dispersion than both initial pollutant concentration and exit velocity. When the exit angle is $15°$, the pollutants tend to spread on the ground region. Crosswind shows a significant effect on the dispersion of the exhaust plume also. It will divert the plume to disperse in the same direction of the wind with limited penetration in the downstream direction.

1. Introduction

Pollutant emissions from motor vehicles have been one of the major air pollution problems, especially in the roadside of mega-cities. They are recognized as one of the most serious health hazards in congested urban areas where road traffic is heavy.

The emissions from a motor vehicle vary under different driving conditions (Tong et al., 2000; Frey et al., 2003). One of the specific driving modes is the idle condition. A motor vehicle may have over 25% of its time spent in the idle mode (Tong et al., 1999). Idling emission is considered more harmful because the pollutants cannot be dispersed by the wake created by a moving vehicle. A specific idle mode is the park-and-wait mode in which the motor vehicle is parked along the street or in a terminal with the engine switched on. It is believed that, due to poor

*Corresponding author. Tel.: +852 27667819;
fax: +852 23654703.
E-mail address: mmcsc@polyu.edu.hk (C.S. Cheung).

combustion conditions inside the engine cylinder when it is operating at idle and the poor dispersion condition when the vehicle is not moving, pollutant concentration will be high around the vehicle. This will pose a threat to the commuters and those waiting for the vehicles. In Hong Kong, due to the close proximity of the traffic to the commuters and shops on both sides of the road, the government has to urge the vehicle operators to switch off the engine while waiting. Despite the significant impact such a mode of operation has on environmental pollution, it has rarely been investigated.

There have been a large number of experimental investigations on the dispersion of pollutants emitted by motor vehicles. However, most of them were carried out either in wind tunnels or on roadside. Wind tunnel experiments were carried out to assess dispersion under the influence of wind, vehicle speed and adjacent structures. Roadside measurements were aimed at examining the pollutant concentrations at various locations, such as highways, roads in residential areas and downtown areas (Knapp and Tejada, 2000; Kittelson et al., 2001). Experimental data were also used to update emission factors for dispersion models and for assessing influence of vehicular emissions in different locations. However, none of these are specifically concerned with the idle operation of motor vehicles. There have also been many numerical studies on the dispersion of the vehicular exhaust plume, taking into account wake generated by the motion of the motor vehicle (Baker, 2001; Kim et al., 2001), and the subsequent dispersion in the street canyon (Chan et al., 2003; Vardoulakis et al., 2003). Again, none of these dealt with the idle operation of motor vehicles. Chan et al. (2001) performed simulation of nitrogen oxides dispersion from a motor vehicle and validated with limited nitrogen oxides data obtained under idle conditions. However, their study was concentrated on the development of a numerical model for simulating the initial dispersion process with emphasis on nitrogen oxides.

The present study thus aims at studying both experimentally and numerically the dispersion of pollutant emitted by a motor vehicle which is operating at idle under idealized and simplified conditions. Experiments were carried out with the emissions from motor vehicle isolated from influence of wind, adjacent motor vehicles and adjacent structures. Despite such conditions not being realistic, they do provide the idealized conditions required for the parametric study, and provide

the first hand data for further study. In the experimental part, the pollutant concentrations in the near field region of the exhaust plume of three motor vehicles were measured, analyzed and compared. The experimental data were also used to test the performance of the numerical model.

Kim et al. (2001) reviewed different categories of models available for modeling the concentration variations in a dispersion plume. In general, these models include the empirical Gaussian models (Kaharabata et al., 2000), the similarity models (Huai and Li, 1993; Obasaju and Robins, 1998), the probability density function models (Ferrero and Anfossi, 1998; Reynolds, 2000; Chan et al., 2001), the k–ε models (Hwang and Chiang, 1988; Sharan and Yadav, 1998; Kim et al., 2001), and the large eddy simulation models (Heinz and van Dop, 1999). Commercial CFD packages are now available for solving fluid flow and dispersion problems (Vardoulakis et al., 2003). For example, Kim et al. (2001) applied the FLUENT CODE to predict the variation of pollutants inside a turbulent plume, using the k–ε eddy dissipation model. Their work showed the benefits of using CFD modeling in applications where dispersion correlations are not required a priori, instead the dispersion coefficients are calculated precisely by solving the turbulent kinetic energy and dissipation equations. Chan et al. (2002) also applied the same code to validate a two-dimensional pollutant dispersion model in an isolated street canyon using a series of standard, Renormalization Group (RNG) and realizable k–ε turbulence models. In the present study, the CFD code PHOENICS 3.3 was used to predict the variation of pollutant concentrations inside the exhaust plume, using the k–ε eddy dissipation model and analyze the effect of various parameters, including initial emission concentration, exhaust exit velocity, tailpipe direction and crosswind speed, on the dispersion of pollutants.

2. Experiment and results

2.1. Experimental condition and facility

The experiments were carried out to gain insight into the evolution of the vehicular pollutants inside the near field region of the exhaust plume of a motor vehicle under idle condition and obtain data for testing the performance of the numerical model.

Experiments were carried out in a semi-enclosed space that has sufficient space for the plume to disperse freely in all directions. The experimental site permitted repeatable measurements in the vehicular exhaust plume under realistic and reproducible conditions. Experiments were carried out when the wind was weak and in the evening to avoid convection current due to the heat of the sun. There was no special control over the temperature and humidity, but care was taken to perform the measurements during stable weather condition. The temperature and relative humidity during the measurements were in the range of 20–22 °C and 50–60%, respectively. The vehicle measured was not moving but its engine was running at low idle condition in order to simulate the situations of vehicles stopping at the red traffic light or waiting for passengers. Three motor vehicles (one 1990 diesel vehicle, one 1997 petrol vehicle and one 1990 petrol vehicle) with brief details shown in Table 1 were used in the experiments. The 1997 petrol vehicle was equipped with a three-way catalytic converter, whereas the 1990 diesel vehicle and the 1990 petrol vehicles did not have any after-treatment device.

During the field measurements, the gaseous pollutant and particulate concentrations inside the near field region of the exhaust plume were measured. The near field region was divided into a number of grid points with the origin at the center of the tailpipe. The separation distance between each grid point is 0.25 m in the x, y and z directions. Measurements were taken at each grid point. In order to eliminate random errors, measurement was made 3 times on one sampling point.

In the experiments, the Scanning Mobility Particle Sizer (SMPS, TSI Model 3934) was used to measure the particulate number concentration and distribution inside the near field region of the exhaust plume. The SMPS was operated to count particulates of 14.3–749 nm using 32 size channels. The SMPS has been commonly used for the investigation of particulate emissions from motor vehicles and engines (Wehner et al., 2004; Mathis et al., 2004). NO_x concentration was measured with a heated chemiluminiscent analyzer (HCLA, California Analytical Instruments, Inc., Model: 400) which has a resolution of 0.1 ppm and a repeatability of 0.5% of full scale. HC was measured with a heated flame ionization detector (HFID, California Analytical Instruments, Inc., Model: 300) which has a resolution of 0.01 ppm and a repeatability of 0.5% of full scale. CO and CO_2 were measured with chemical cells (Anapol ag, Exhaust Emissions Analyzer, EU-200/3/4). The instrument has a resolution of 0.01% for CO_2 and 0.5 ppm for CO. The gas analyzers were calibrated with standard gases before conducting the measurements, with the HC analyzer calibrated against propane. The gas analyzers are used for measuring raw gases with resolutions on the ppm level. Hence the experimental results shown are limited to the ppm level.

2.2. Results and discussion

In the experiments, the test vehicles were operated under idle condition on the test site and experienced no prevailing wind. The Cartesian coordinate system (x, y, z) is fixed on the ground, as shown in Fig. 1. The origin of the coordinate system is on the centerline of the tailpipe exit of the vehicle. The height of the tailpipe above the ground is H.

The mean pollutant concentrations are shown in the figures. For the gaseous pollutants, the mean values were the average of three measurements with each measurement lasting 4 min. The maximum standard deviation of the measurements was less than 10% of the mean values. For the particulate number concentrations and size distribution, three scans were taken at each sampling point. The maximum difference between the mean geometric mean diameter and the mean total concentration of
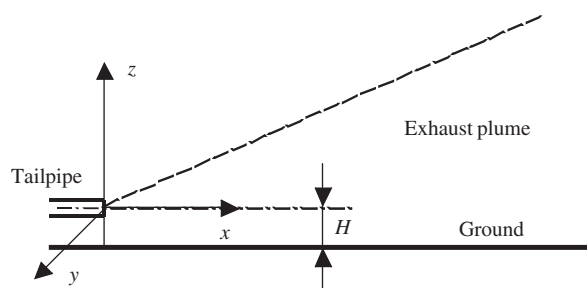
Table 1
Description of the vehicles and engines

Test vehicle	Engine	Year	Displacement	Idle rpm
Vehicle A	Diesel	1990	2779 cm³	640
Vehicle B	Petrol	1997	1493 cm³	720
Vehicle C	Petrol	1990	1952 cm³	700

Fig. 1. Schematic of the Cartesian coordinate system and vehicular exhaust plume geometry.

the three scans and those of individual scan were less than 12% of the mean value.

The NO_x and CO concentrations, as well as the particulate concentrations and size distributions, at different sampling points inside the exhaust plume of the 1990 diesel vehicle are shown in Figs. 2–4.

Fig. 2(a) shows that the concentrations of NO_x and CO decreased rapidly along the downstream distance of the vehicular exhaust plume. The concentrations of NO_x and CO at the tailpipe exit were 140 and 60 ppm by volume, respectively, and dropped exponentially to less than 1 ppm, within a distance of 3.0 m or so downstream. Fig. 2(a) also compares the NO_x concentrations at $z = 0.0$, 0.5 and 1.0 m above the centerline. At a height of 0.5 m, the NO_x concentration increased from the background concentration at $x = 0$ to a peak value of about 40 ppm at $x = 0.5$ m and then dropped quickly to less than 1 ppm. At a height of 1.0 m,
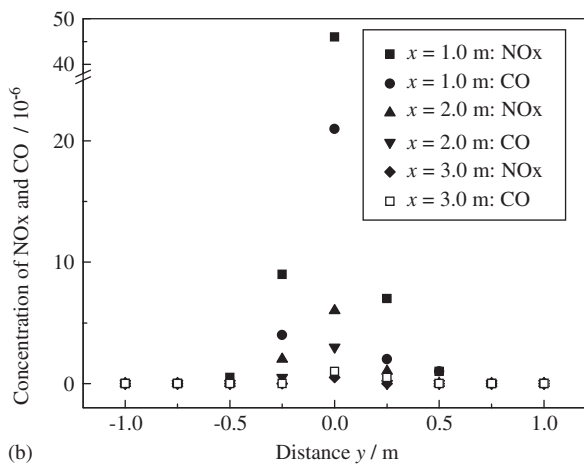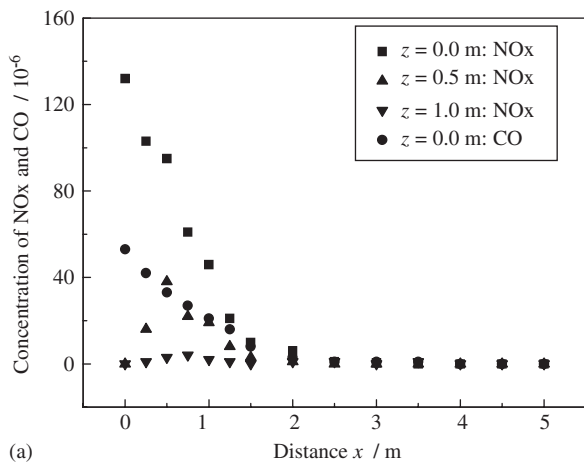

(a)

(b)

Fig. 2. Concentrations of NO_x and CO at different sampling points for vehicle A. (a) $y = 0.0$ m; (b) $z = 0.0$ m.
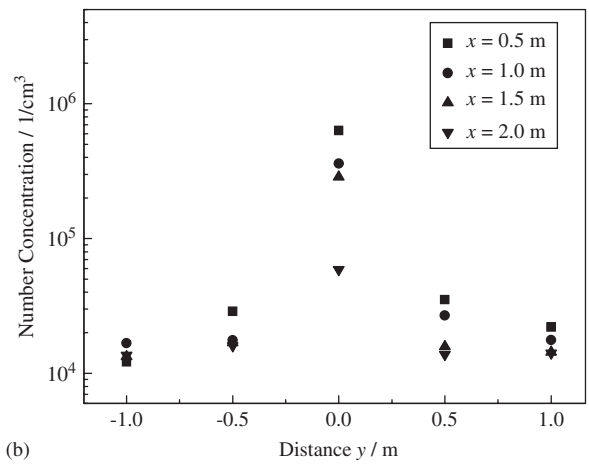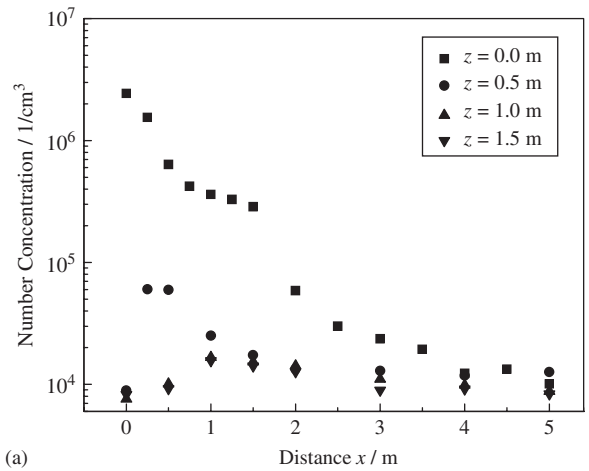

(a)

(b)

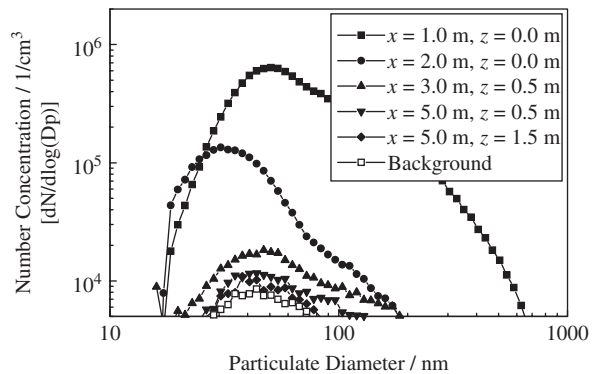Fig. 3. Particulate number concentration at different sampling points for vehicle A. (a) $y = 0.0$ m; (b) $z = 0.0$ m.

Fig. 4. Size distributions of particulate at different locations for vehicle A.

the NO_x concentration was always very low. The results indicated that at calm conditions, upward dispersion was not significant at levels above 1.0 m.

Fig. 2(b) shows the horizontal dispersion at three different downstream distances. The concentrations of NO_x and CO diffused to less than 1 ppm within a horizontal distance of 0.5 m from the centerline of the exhaust plume. It can be observed from Fig. 2(b) that the distributions of NO_x and CO concentrations were not symmetrical about the center of the plume, probably due to the influence of the prevailing environment.

Fig. 3 shows the particulate number concentrations at different locations in the exhaust plume. It is observed that, due to rapid dilution with ambient air, the concentration of particulates decreased rapidly along the centerline of the vehicular exhaust plume, in the horizontal direction and in the vertical direction. The concentration dropped to the background aerosol concentration within a distance of 3.0 m or so downstream of the exhaust plume and within a horizontal distance of approximately 1.0 m from the centerline of the plume. The dispersion behaviors of the particulate number concentration inside the exhaust plume were similar to that of the gaseous pollutants.

The size distribution of the particulate at different locations is presented in Fig. 4, with the background aerosol size distribution shown for comparison. The results show that the size distributions of the particulate in the exhaust plume were almost unimodal with peaks in the size range of 40–50 nm for the vehicle measured. Besides the rapid reduction of number concentration, there was also a reduction in the range of particle size as the particulates were dispersed. The size distribution was moving towards that of ambient air, indicating the strong influence of ambient air on the dilution process.

The concentrations of NO_x, CO, HC and the number concentration of particulates in the exhaust plume for the three motor vehicles are presented in Fig. 5. The results show that the diesel vehicle (vehicle A) had the highest level of NO_x concentration and particulate number concentration, while the 1997 petrol vehicle (vehicle B) had the lowest level of these pollutants. On the other hand, the diesel vehicle had the lowest concentrations of CO and HC emissions while the 1990 petrol vehicle had the highest emissions of these two pollutants. It can be concluded that there are significant differences of pollutant concentrations in the exhaust plume for different vehicles under idle condition, and the difference depends on the type of the vehicle, the vehicle technology level and the conditions of the

vehicle. However, despite the initial difference in emissions concentrations, the difference reduced to a very low value at about 3.0 m downstream of the exhaust outlet for the gaseous pollutants and particulates.

Figs. 6(a) and (b) compare the particulate size distributions for the three motor vehicles at the downstream distance of 0.5 and 1.0 m, respectively, along the centerline of the plume, together with the size distribution of the background aerosol. Over the whole spectrum of particle size, the diesel vehicle emitted much more than the petrol vehicles; while the 1990 petrol vehicle emitted much more than the 1997 petrol vehicle especially for particles below 100 nm. The particulate size distributions of the diesel vehicle were nearly lognormal with mean diameters ranging from 60 to 120 nm, whereas for petrol vehicles the size distributions tended to be asymmetric and had smaller mean diameters of 40–80 nm. Compared with the 1990 petrol vehicle, the mean diameter of the particulate of the 1997 petrol vehicle was larger while the particulate number was lower. It can be concluded that under idle operation, all the three vehicles emitted particulates over the ambient level.

3. Numerical model and discussion

3.1. Analytical model and simulation conditions

Due to the difference in the nature of the gaseous pollutants and particulate, their concentration distributions inside the exhaust plume should be different. In this paper, we will limit our simulations to gaseous pollutants, and the dispersion of CO is selected for parametric study.

The Cartesian coordinate system (x, y, z) used in the numerical analysis is shown in Fig. 1, with the origin of the coordinate system on the ground. The pollutants are emitted from the exhaust tailpipe of a vehicle at a certain flow rate, and dispersed into the atmosphere. This process can be considered as a jet and boundary layer problem (Chan et al., 2001). For such a problem, Kim et al. (2001) has demonstrated that the k–ε eddy dissipation model can be used to analyze the physical phenomena of the dispersion of a turbulent plume emitted by a vehicle accurately.

In order to describe the process of the dispersion of exhaust pollutants in the atmosphere accurately, the effects of turbulent mixing, convection, diffusion, temperature variations and species transport
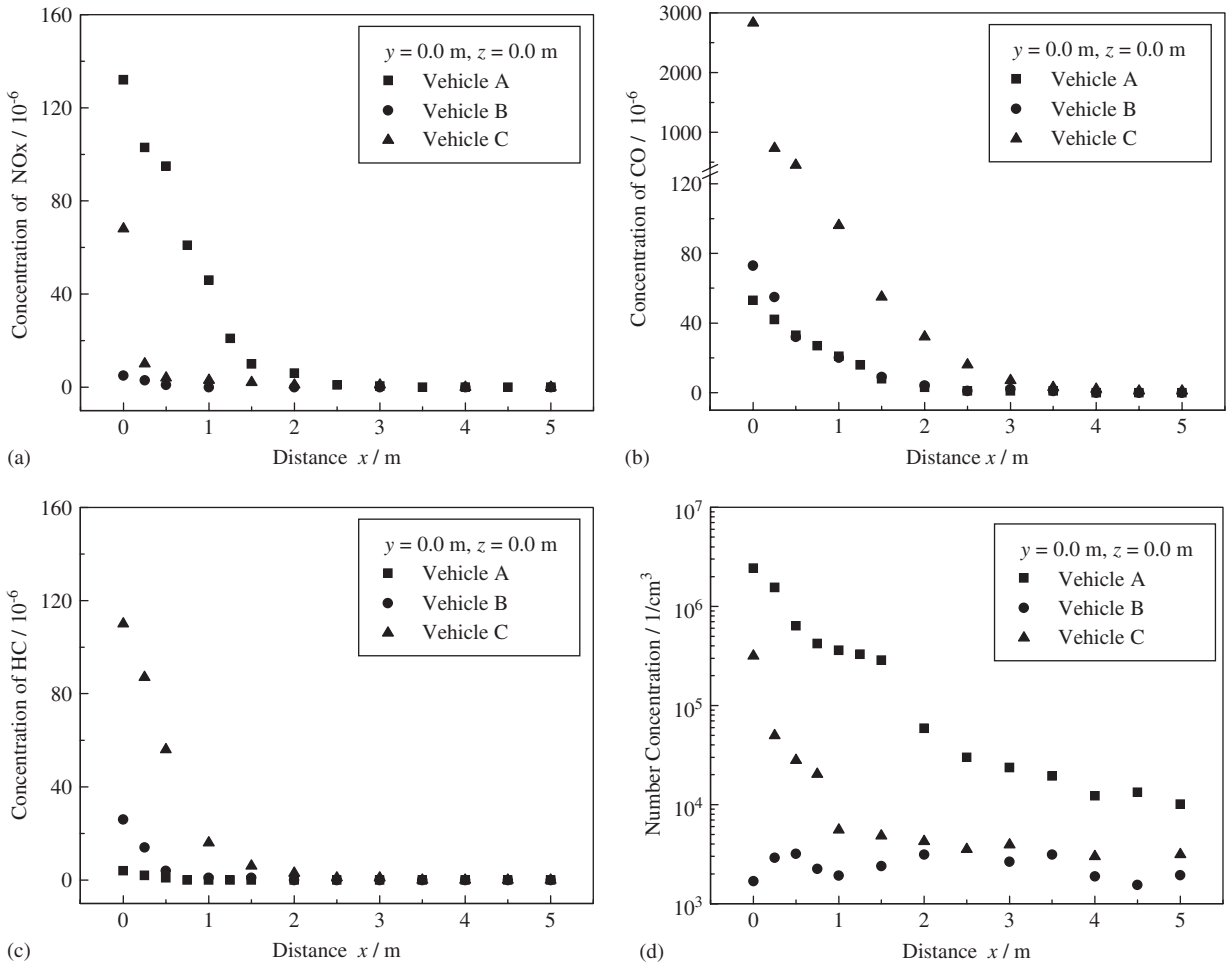
Fig. 5. Comparison of NO$_x$, CO, HC and particulate number concentration in exhaust flume of different vehicles.

must be considered. The gas flow in the above configuration can be described by the time-averaged equations of global mass, momentum, enthalpy and species mass fractions. For closure, the standard k–ε turbulence closure was used in the current CFD simulation. As such, the governing equations for the problem studied can be written as (Kim et al., 2001):

Continuity equation:

$$\frac{\partial}{\partial x_i}(\rho \overline{u_i}) = 0, \tag{1}$$

where ρ is the fluid average density; $\overline{u_i}$ is the mean velocity component in the direction of coordinate x_i.

Momentum equation:

$$\frac{\partial}{\partial x_j}\left[\rho \overline{u_j u_i} + p\delta_{ij} - \mu\left(\frac{\partial \overline{u_i}}{\partial x_j} + \frac{\partial \overline{u_j}}{\partial x_i} - \frac{2}{3}\frac{\partial \overline{u_k}}{\partial x_k}\,\delta_{ij}\right)\right]$$
$$+ \rho g_i + \frac{\partial}{\partial x_j}(\rho \overline{u_j' u_i'}) = 0, \tag{2}$$

where p is the fluid average pressure, μ is the fluid laminar viscosity, g_i is the gravitational acceleration in the direction of coordinate z_i, when $i = j$ the operator $\delta_{ij} = 1$ and when $i \neq j$ operator $\delta_{ij} = 0$. In this study, the Reynolds stresses are modeled using the two-equation k–ε model. Hence, the Reynolds stresses term in Eq. (2) can be written as

$$-(\rho \overline{u_j' u_i'}) = \mu_t\left(\frac{\partial \overline{u_i}}{\partial x_j} + \frac{\partial \overline{u_j}}{\partial x_i} - \frac{2}{3}\frac{\partial \overline{u_k}}{\partial x_k}\,\delta_{ij}\right), \tag{3}$$

where μ_t is the fluid turbulent viscosity and can be expressed as

$$\mu_t = c_\mu k^2/\varepsilon, \tag{4}$$

where c_μ is a constant of the model. k and ε can be solved by the turbulent energy (k) equation and the turbulent dissipation (ε) equation:
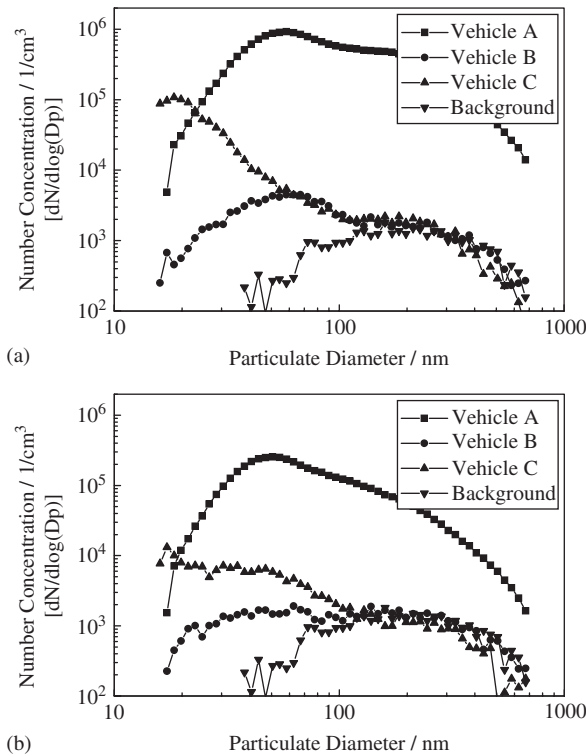
Fig. 6. Size distributions of particulate for different vehicles. (a) $x = 0.5\,\text{m}$, $y = 0.0\,\text{m}$, and $z = 0.0\,\text{m}$; (b) $x = 1.0\,\text{m}$, $y = 0.0\,\text{m}$ and $z = 0.0\,\text{m}$.

Turbulent energy (k) *equation*:

$$\frac{\partial}{\partial x_j}(\rho \overline{u_j} k) - \frac{\partial}{\partial x_j}\left(\Gamma_k \frac{\partial k}{\partial x_j}\right)$$
$$- \mu_t \frac{\partial \overline{u_i}}{\partial x_j}\left(\frac{\partial \overline{u_i}}{\partial x_j} + \frac{\partial \overline{u_j}}{\partial x_i}\right) + \rho\varepsilon = 0. \qquad (5)$$

Turbulent dissipation (ε) *equation*:

$$\frac{\partial}{\partial x_j}(\rho \overline{u_j} \varepsilon) - \frac{\partial}{\partial x_j}\left(\Gamma_\varepsilon \frac{\partial \varepsilon}{\partial x_j}\right)$$
$$- C_1 \frac{\varepsilon}{k} \mu_t \frac{\partial \overline{u_i}}{\partial x_j}\left(\frac{\partial \overline{u_i}}{\partial x_j} + \frac{\partial \overline{u_j}}{\partial x_i}\right) + C_2 \rho \frac{\varepsilon^2}{k} = 0, \qquad (6)$$

where C_1 and C_2 are constants of the model, Γ_k and Γ_ε can be determined via Boussinesq approximations.

Energy conservation equation:

$$\frac{\partial}{\partial t}(\rho h) + \frac{\partial}{\partial x_i}(\rho u_i h)$$
$$= \frac{\partial}{\partial x_i}\left[(k + k_t)\frac{\partial T}{\partial x_i}\right] - \frac{\partial}{\partial x_i}\sum (h_{\bar{i}} J_{\bar{i},i})$$
$$+ \frac{Dp}{Dt} + \tau_{ik}\frac{\partial u_i}{\partial x_k} = 0, \qquad (7)$$

where h is the static enthalpy, k is the molecular conductivity, k_t is the effective molecular conductivity and can be expressed as $k_t = \mu_t/\text{Pr}_t$, $J_{i',i}$ is the diffusion flux of the ith chemical species due to the concentration gradients of the species.

Species transport equation:

$$\frac{\partial}{\partial t}(\rho C_i) + \frac{\partial}{\partial x_i}(u_i C_i) = -\frac{\partial J_{\bar{i},i}}{\partial x_i} + R_i, \qquad (8)$$

where C_i is the mean concentration of the ith species, and R_i is the source term due to the chemical reactions. The chemical reactions among different species are not considered.

In the process of simulation, the dimensions of the integrated domain were taken to be $15\,\text{m} \times 6\,\text{m} \times 3\,\text{m}$. The diameter of the tailpipe was $0.03\,\text{m}$, and the height of the tailpipe above the ground was $0.3\,\text{m}$. The external boundary of the integrated domain was defined as free stream boundary. The exit velocity of $4.8\,\text{m/s}$ used in the
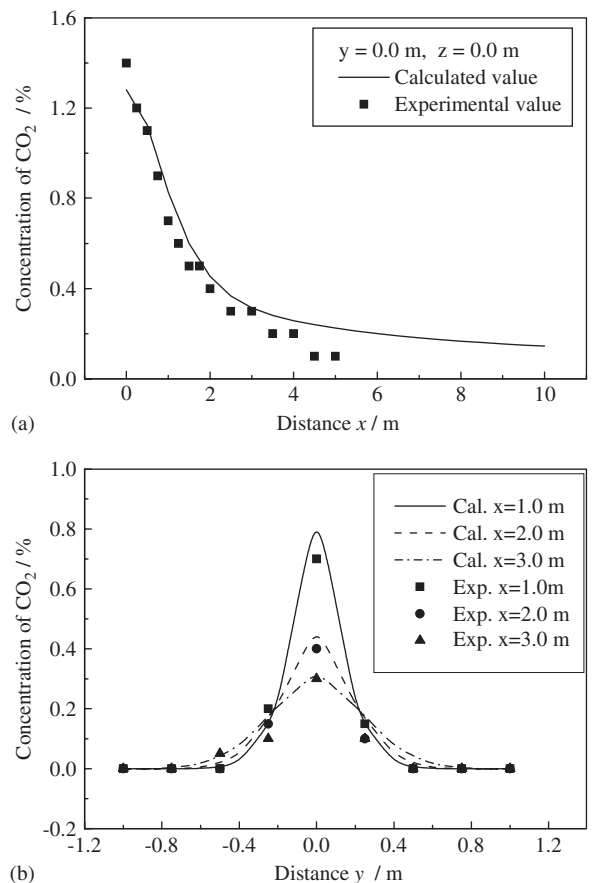

Fig. 7. Comparison of CO_2 concentration between the experimental data and simulated results. (a) $y = 0.0\,\text{m}$; (b) $z = 0.0\,\text{m}$.

simulation was selected with reference to the measured values while the CO concentrations were selected to be less than 5000 ppm which is the maximum idle CO concentration allowable for 1992 and later vehicles in Hong Kong. The atmospheric temperature and the exhaust gas temperature at the tailpipe exit were chosen as 293 and 380 K, respectively. The transport equations described in this section were discretized by the finite volume method using a hybrid scheme and the computations were performed inside the computation space using the commercial CFD package PHOE-NICS 3.3.

A specific goal of this section is to study the effect of parameters such as emission concentration, exhaust exit velocity, tailpipe exit direction and

crosswind strength on the dispersion of the exhaust plume.

3.2. Analysis and discussion

Kim et al. (2001) validated the k–ε eddy dissipation model by comparing the relative concentration of CO_2, dilution ratio and temperature variations inside the exhaust plume predicted by the CFD model with experimental data obtained from wind tunnel tests. Their predicted results showed an excellent agreement with the experimental data. In this paper, we also used the simulated and measured CO_2 concentrations for validation. Fig. 7(a) compares the experimental and simulated results along the centerline of the exhaust plume for vehicle A. It
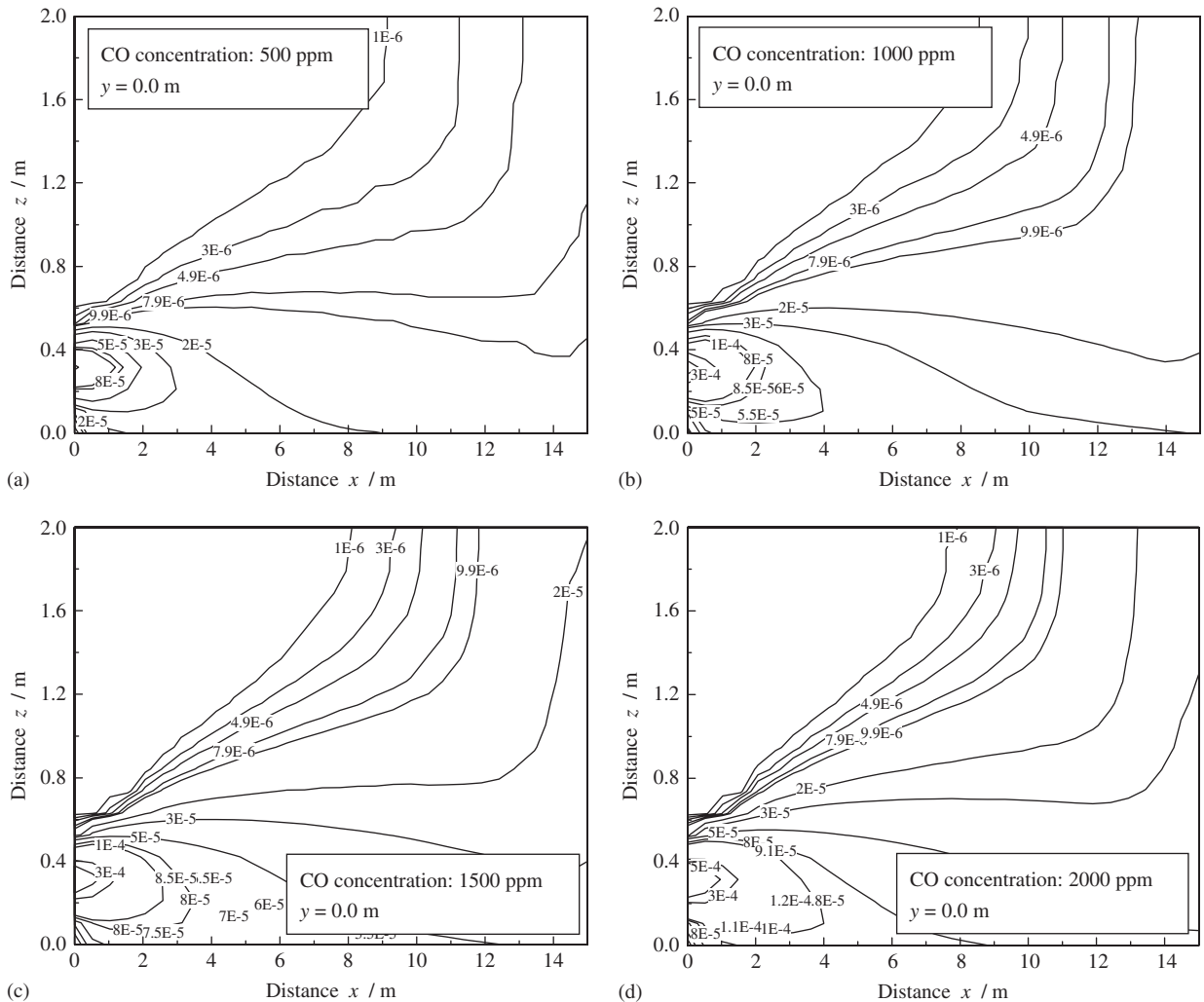

Fig. 8. Distribution of CO concentration under different initial CO emission concentration (exit velocity: $4.8\,\mathrm{m\,s^{-1}}$).
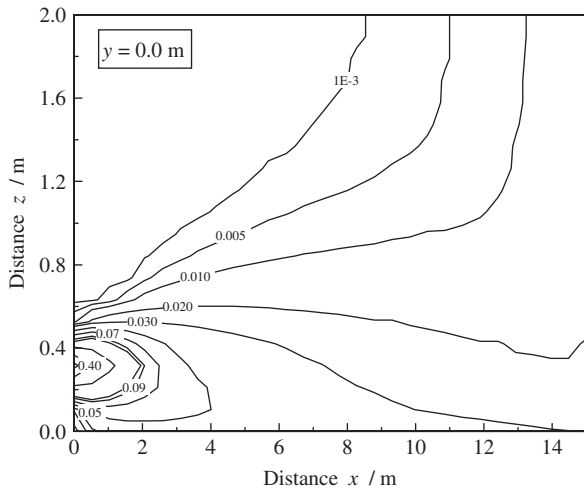
Fig. 9. Distribution of CO relative concentration under different initial CO emission concentration (exit velocity: $4.8\,\mathrm{m\,s^{-1}}$).

can be observed that the simulated results are slightly higher than the experimental data and the CO_2 concentration persists longer in the simulated plume than the actual plume. However, the simulation correctly predicts the exponential decay of the CO_2 concentration along the centerline of the plume. Fig. 7(b) also shows that the simulated results match well the dispersion of the pollutant in the horizontal direction, at three different sections of the plume. These simulated results reflect that the numerical model can predict well the dispersion of the pollutants in the exhaust plume.

The model was further applied for parametric study of the effect of initial pollutant concentration, exit velocity, exit angle and crosswind on the dispersion of the CO in the exhaust plume.

The effects of initial pollutant concentration are shown in Figs. 8–10. The initial CO concentrations correspond to those of well-maintained petrol vehicles. Fig. 8 presents the contour of CO concentration distribution in the section x–z for four different CO emission concentrations under the same exit velocity of $4.8\,\mathrm{m\,s^{-1}}$. For comparison, the lowest CO concentration considered is 1×10^{-6}. It can be seen from Fig. 8 that the concentration dropped rapidly in a small region around the emission source. Subsequently, pollutant dispersion is much less intense. For example, with an exit concentration of 500 ppm, the centerline concentration drops to about 20 ppm in the first 5 m and then drops to about 10 ppm in another 5 m. The results
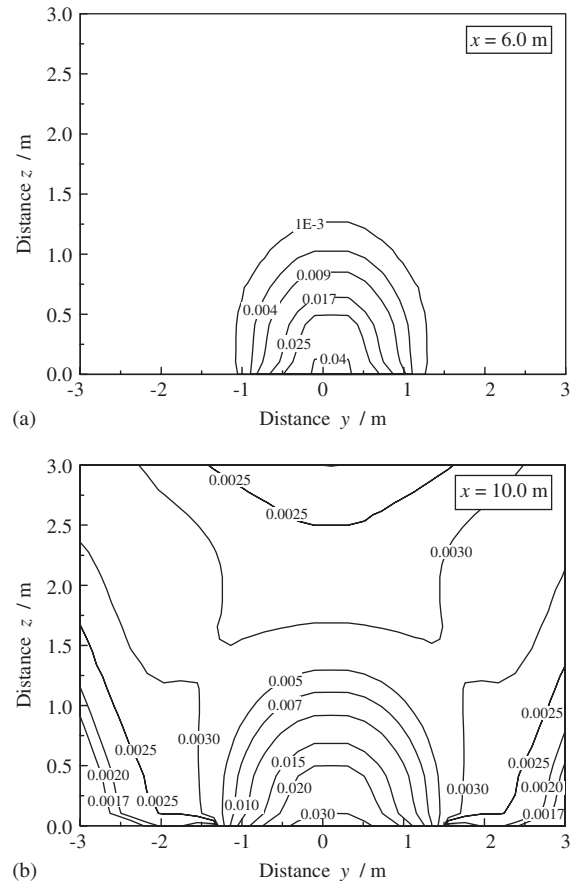
Fig. 10. Distribution of CO relative concentration in the section y–z for downstream distances of 6 and 10 m (exit velocity: $4.8\,\mathrm{m\,s^{-1}}$).

match with the general decay of CO concentration shown in experimental results except that the simulated results decay much slower in the later stage of dispersion. The higher the initial emission concentration, the farther the pollutants disperse along the centerline of the vehicular exhaust plume. The pollutant concentration at a fixed location increases almost linearly with the increase in emission concentration. Due to the momentum of the plume, upward dispersion is significant only at 6 m downstream and beyond.

The contours for different emission concentrations are quite similar. This similarity is expected since only the concentration gradient is varied in all these cases. Fig. 9 presents the distribution of CO relative concentration. The distribution of CO relative concentration is identical for different initial CO emission concentration.

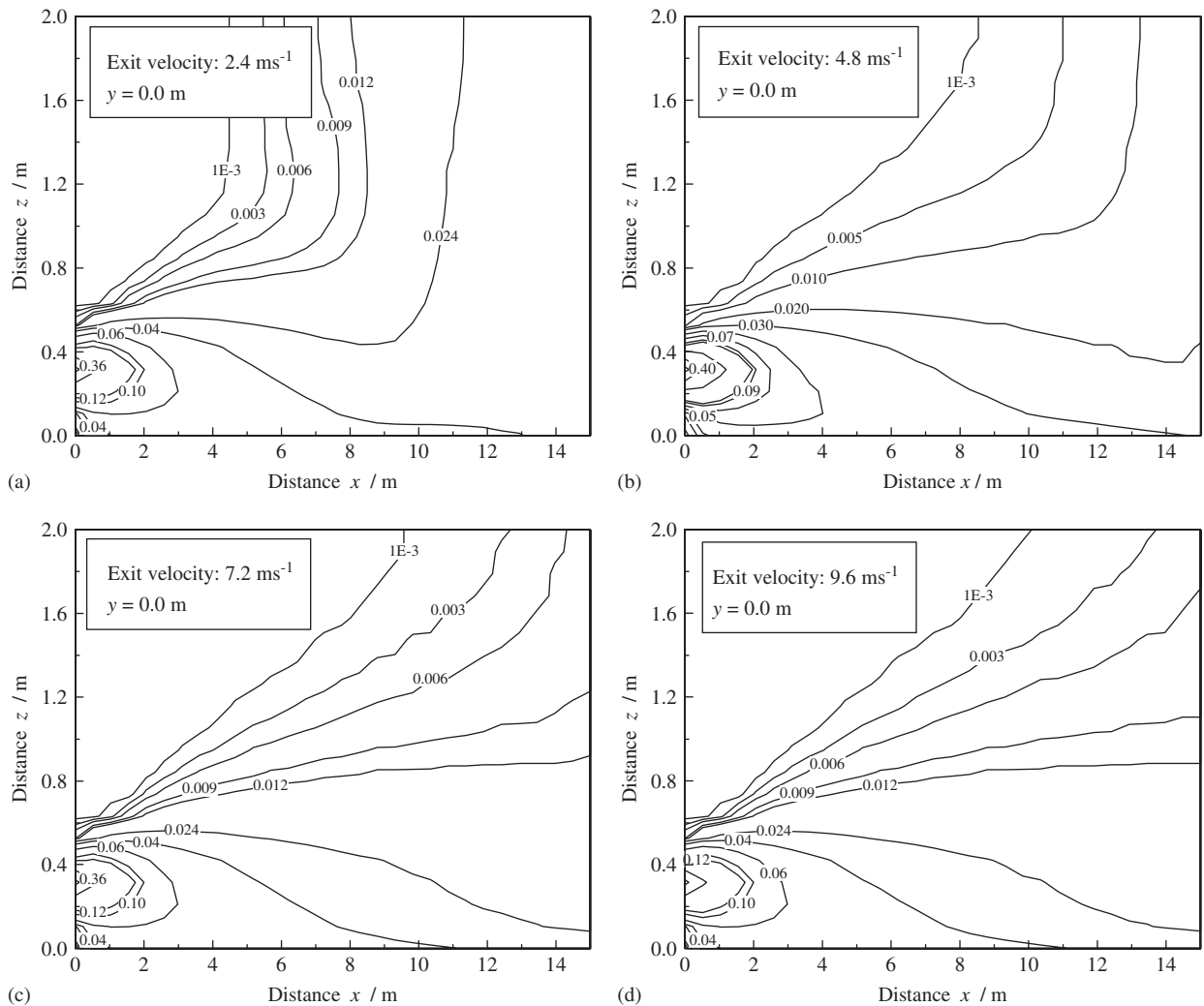Fig. 11. Distribution of CO relative concentration under different exit velocities.

Fig. 10 presents the contour of CO relative concentration distribution in the y–z section for downstream distances of 6 and 10 m along the centerline of the vehicular exhaust plume, with an exit velocity of $4.8\,\mathrm{m\,s^{-1}}$. The figure shows that at a downstream distance of 6 m, the dispersion is confined to a semicircle of less than 1.5 m in diameter and spreads to the whole computational domain at the downstream distance of 10 m. In the former case, commuters along both sides of the vehicle will be affected to a lesser extent, while in the latter case, they will be significantly affected.

The effects of exit velocities on the dispersion are shown in Figs. 11 and 12. The exit velocity of $4.8\,\mathrm{m\,s^{-1}}$ was chosen based on the actual exit velocities of the three vehicles tested in this study.

The other exit velocities were chosen to reflect the change when the exit velocity was reduced to half, increased by 50% and increased by 100%. Fig. 11 shows the contour of CO relative concentration distribution in the x–z section under different exit velocities. The concentration of CO decreases rapidly within a small distance of about 2 m in the downstream direction, and within this distance, there is no obvious difference in the CO concentration distributions under different exit velocities. Further downstream, the CO concentration decreases gradually, being slightly faster along the centerline of the exhaust plume when the exit velocity is higher. It can be observed that there is only slight difference between the two diagrams on exit velocities of 7.2 and $9.6\,\mathrm{m\,s^{-1}}$. On the other
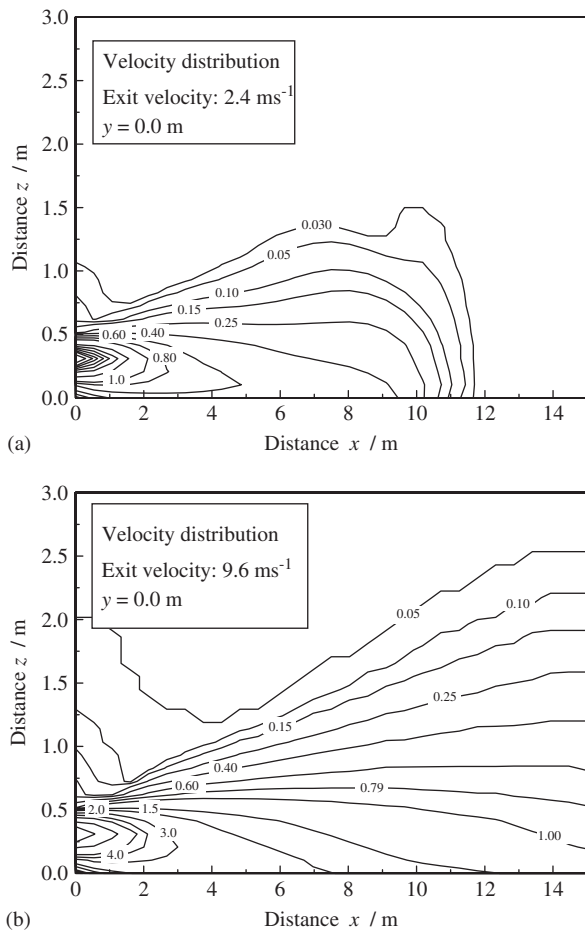
Fig. 12. Distribution of flow velocity under different exit velocities.

hand, within the computational domain, strong upward dispersion of CO occurs at the lower velocities of 2.4 and 4.8 m s^{-1}. The strong upward dispersion occurs earlier at lower exit velocity. Fig. 12, which shows the x–y section velocity contours under two exit velocities of 2.4 and 9.6 m s^{-1}, is plotted for further investigation of the upward dispersion. A comparison with the corresponding CO relative concentration contours in Fig. 11 shows that the pollutant will be dispersed upward rapidly when the local velocity is approaching zero. For example, the upward dispersion in Fig. 11(a) starts at about $x = 4$ m and $z = 1.2$, while in Fig. 12(a), the velocity becomes negligible at the same location. From these observations, we can conclude the two effects of the exit velocity on the dispersion. First, at a higher exit velocity, the higher momentum of the jet will ensure deeper penetration of the jet downstream. Second, at a lower velocity, the

momentum will die down early, thus facilitating vertical dispersion of the jet.

Fig. 13 presents the contour of CO relative concentration distribution in the section x–z under different exit angles to the horizontal, at an exit velocity of 4.8 m s^{-1}. The angles were chosen to reflect feasible exit arrangements. It can be seen that the change in exit direction has a stronger influence on the dispersion of pollutant in the exhaust plume than that due to the change in initial pollutant concentration or exit velocity, by directing the gas towards the ground. At an angle of 15° relative to the horizontal direction, the dispersion region is limited to a thin layer above the ground. However, when the angle is increased to 30° or 45°, the stronger interaction between the gas flow and the ground causes an upward dispersion of the plume. The larger the angle, the earlier the pollutant dispersed in the vertical direction. When the angle is 30°, the downstream distance at which the pollutant is dispersed in the vertical direction is about 10 m, and when the angle is 45°, it is only 7 m. It can be seen from the simulated results that vertical dispersion can be confined or controlled by the exit angle to the horizontal.

Crosswind can affect the dispersion of the exhaust plume in the transverse region downstream of the vehicle. The effect of crosswind on the dispersion of the exhaust pollutant is shown in Fig. 14. This figure presents the contour of CO relative concentration in the section x–y downstream of the vehicle under four different crosswind speeds, with an exhaust exit velocity of 4.8 m s^{-1}. The crosswind plays a significant role in the development of the exhaust plume. Even when the crosswind speed is as small as 0.1 m s^{-1}, the exhaust plume is confined to disperse on the leeward side of the plume, as shown in Fig. 14(a). At higher crosswind speed, the plume is dispersed mainly in the crosswind direction rather than in the downstream direction. The stronger the crosswind, the shorter the plume is able to penetrate downstream. For example, at a crosswind velocity of 2 m s^{-1}, the plume does not affect the downstream region beyond a distance of about 3 m. It can be concluded that the crosswind will divert the plume to disperse in the direction of the wind rather than in the downstream direction.

4. Conclusions

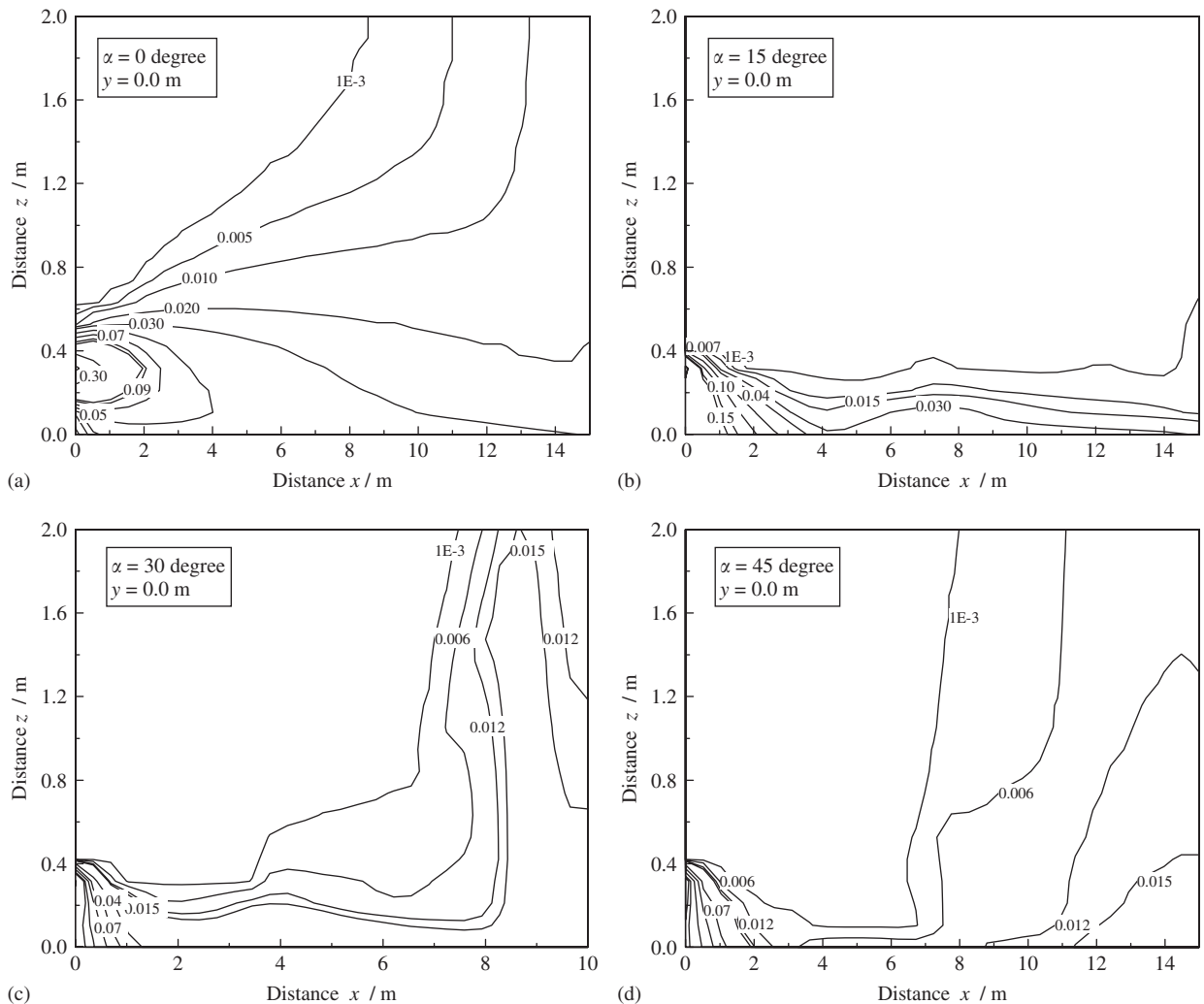Idling emissions of a vehicle is considered more harmful on human health because the pollutants

Fig. 13. Distribution of CO relative concentration under different tailpipe exit direction (exit velocity: $4.8\,\mathrm{m\,s^{-1}}$).

cannot be dispersed by the wake created by a moving vehicle. This paper attempts to study, both experimentally and numerically, the dispersion characteristics of the exhaust plume when a vehicle is operating under idle condition by considering the dispersion of the exhaust plume of a vehicle from its point of emission to some distance downstream.

Three motor vehicles were involved in the experimental investigation: a 1990 diesel vehicle, a 1997 petrol vehicle and a 1990 petrol vehicle. The three vehicles emitted different concentrations of gaseous pollutants of CO, HC and NO_x and particulate but all pollutants decayed almost to the background concentrations within a distance of 3 m along the centerline from the emission source,

within a distance of 1 m from both sides of the centerline and to a height of 1 m. The results also show that the contributions of petrol vehicles to the concentration of particulates inside the exhaust plume cannot be neglected, especially for small size particulates. In the exhaust plume near the tailpipe, the particulate size distributions of the diesel vehicle were nearly lognormal with mean diameters ranging from 60 to 120 nm, whereas for the petrol vehicles the size distributions tended to be asymmetric and had smaller mean diameters of 40–80 nm. The experimental results also show that the 1997 petrol vehicle had the lowest emissions at idle. Hence, it helps reduce the impact to commuters if older vehicles are replaced with newer ones complying with the latest emissions standard.

Fig. 14. Distribution of CO relative concentration under different crosswind speeds (exit velocity: $4.8 \, \mathrm{m \, s^{-1}}$).

In this paper the CFD code PHOENICS 3.3 was used to analyze the dispersion of gaseous pollutant, using the k–ε eddy dissipation model. The model was validated with CO_2 concentrations measured experimentally. The model was able to simulate closely the experimental results close to the source but the simulated results took a longer distance to decay to ambient values. The model was then applied to investigate the effects of initial pollution concentration, exit velocity, exit direction and crosswind intensity on the dispersion. The initial pollutant concentration will increase the local concentrations close to the emission source but the pattern of dispersion remains the same. The exit velocity will increase the momentum of the jet, resulting in a deeper penetration downstream. At

low exit velocity, the downstream penetration will be weakened while upward dispersion becomes more dominant. The exit angle has stronger influence on pollutant dispersion than both initial pollutant concentration and exit velocity. When the exit angle is $15°$, the pollutants tend to spread on the ground region. At $30°$ and $45°$, there is a stronger interaction between the gas flow and ground, resulting in an upward deflection of the gas flow; the larger the angle, the earlier the pollutants dispersed in the vertical direction. The angle of the tailpipe exit can play an important role in limiting the dispersion of pollutants in the vertical direction. Crosswind shows a significant effect on the dispersion of the exhaust plume also. It will divert the plume to disperse in the same direction of the wind

with limited penetration in the downstream direction; the stronger the cross wind, the weaker the downstream dispersion.

Both the experimental results and numerically simulated result show the build up of gaseous and particulate pollutants in the wake of a motor vehicle operating under idle conditions. The concentrations of the pollutants are affected by the initial concentration of the pollutant concerned and the exit velocity. At low exit velocity, the pollutants concentrations tend to be higher closer to the source of emission. Higher exit velocity will help to disperse the pollutants further downstream. The dispersion is strongly affected by the exit angle. An appropriate exit angle can help to limit dispersion in the vertical direction. The simulated results show that if upward dispersion in the vicinity of a vehicle is to be avoided to reduce the impact to commuters, the exit angle and the exit velocity can be adjusted as far as it is practical to increase dilution of the pollutants at the ground level.

Acknowledgments

References

Baker, C.J., 2001. Flow and dispersion in ground vehicle wakes. Journal of Fluids and Structures 15, 1031–1060.

Chan, A.T., Au, W.T.W., So, E.S.P., 2003. Strategic guidelines for street canyon geometry to achieve sustainable street air quality—Part II: multiple canopies and canyons. Atmospheric Environment 37, 2761–2772.

Chan, T.L., Dong, G., Cheung, C.S., Leung, C.W., Wong, C.P., Hung, W.T., 2001. Monte Carlo simulation of nitrogen oxides dispersion from a vehicular exhaust plume and its sensitivity studies. Atmospheric Environment 35, 6117–6127.

Chan, T.L., Dong, G., Leung, C.W., Cheung, C.S., Hung, W.T., 2002. Validation of a two-dimensional pollutant dispersion model in an isolated street canyon. Atmospheric Environment 36, 861–872.

Ferrero, E., Anfossi, D., 1998. Comparison of PDFs, closure schemes and turbulence parameterizations in Lagrangian stochastic models. International Journal of Environment and Pollution 9, 384–410.

Frey, H.C., Unal, A., Rouphail, M., Colyar, J.D., 2003. On-road measurement of vehicle emissions using a portable instru-

ment. Journal of the Air and Waste Management Association 53, 992–1002.

Heinz, S., van Dop, H., 1999. Buoyant plume rise described by a Lagrangian turbulence model. Atmospheric Environment 33 (13), 2031–2043.

Huai, W., Li, W., 1993. Similarity solutions of round jets and plumes. Applied Mathematics and Mechanics (English Edition) 14, 649–658.

Hwang, R.R., Chiang, T.P., 1988. Numerical simulation on turbulent buoyant jets in a flowing stratified ambient. Proceedings of the ASME International Mechanical Engineering Congress and Exposition, vol. 247, November 15–20, 1998, pp. 85–88.

Kaharabata, S.K., Schuepp, P.H., Desjardins, R.L., 2000. Source strength determination of a tracer gas using an approximate solution to the advection-diffusion equation for microplots. Atmospheric Environment 34, 2343–2350.

Kim, Dong-Hee, Mridul, G., Dinesh, G., 2001. On the prediction of concentration variations in a dispersing heavy-duty truck exhaust plum using k–ε turbulent closure. Atmospheric Environment 35, 5267–5275.

Kittelson, D.B., Watts, W.F., Johnson Jr., J.P., 2001. Fine particle (nanoparticle) emissions on Minnesota highways. Final Report 1999–2001, MN/RC-2001-12, Minnesota Department of Transportation, performed by Department of Mechanical Engineering, University of Minnesota.

Knapp, K.T., Tejada, S.B., 2000. Central Carolina vehicle particulate emission study. Final Report, US Environmental Protection Agency MD-46.

Mathis, U., Kaegi, R., Mohr, M., Zenobi, R., 2004. TEM analysis of volatile nanoparticles from particle trap equipped diesel and direct-injection spark-ignition vehicles. Atmospheric Environment 38 (26), 4347–4355.

Obasaju, E.D., Robins, A.G., 1998. Simulation of pollution dispersion using small scale physical models—an assessment of scaling options. Environmental Monitoring and Assessment 52, 239–254.

Reynolds, A.M., 2000. Representation of internal plume structure in giffords meandering plume model. Atmospheric Environment 34, 2539–2545.

Sharan, M., Yadav, A.K., 1998. Simulation of diffusion experiments under light wind, stable conditions by a variable k-theory model. Atmospheric Environment 32, 3481–3492.

Tong, H.Y., Hung, W.T., Cheung, C.S., 1999. Development of a driving cycle for Hong Kong. Atmospheric Environment 33, 2323–2335.

Tong, H.Y., Hung, W.T., Cheung, C.S., 2000. On-road motor vehicle emissions and fuel consumption in urban driving conditions. Journal of the Air and Waste Management Association 50, 543–554.

Vardoulakis, S., Fisher, B.E.A., Pericleous, K., Gonzalez-Flesca, N., 2003. Modelling air quality in street canyons: a review. Atmospheric environment 37, 155–182.

Wehner, B., Philippin, S., Wiedensohler, A., Scheer, V., Vogt, R., 2004. Variability of non-volatile fractions of atmospheric aerosol particles with traffic influence. Atmospheric Environment 38 (36), 6081–6090.